JOURNAL OF MATERIALS SCIENCE 9 (1974) 270–278

Crack propagation and failure prediction in silicon nitride at elevated temperatures

A. G. EVANS, S. M. WIEDERHORN
National Bureau of Standards, Washington DC, USA

A technique for studying high temperature crack propagation in ceramic materials is developed. The technique is used to obtain relationships between the crack propagation rate and the stress intensity factor for hot-pressed silicon nitride up to 1400° C. The data are then used to develop proof test diagrams which give values for the safe working stress levels for this material after proof testing (or any other flaw detection procedure).

1. Introduction

Silicon nitride has emerged as a material with outstanding potential for high temperature structural applications [1]. High strength (~ 1000 MN m^{-2}) can be attained – using hot-pressing techniques in particular – and this strength is retained to relatively high temperatures (~ 1000° C). At the temperatures where ceramic materials need to operate to gain the requisite strength advantage over metallic materials, however (i.e. above ~ 1100° C), some strength degradation usually occurs (Fig. 1). It is clearly of paramount importance to characterize the strength in this temperature regime to establish effective operational stress levels for component design. The primary objective of this paper is the evaluation of safe working stresses for hot pressed silicon nitride.

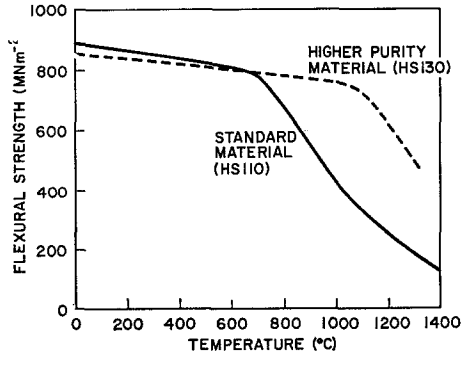

Figure 1 The temperature dependence of the three point flexural strength of two hot-pressed silicon nitrides, supplied by the Norton Company, in an orientation orthogonal to the hot-pressing direction.

Recent observations have implied that the high temperature strength degradation is due to the onset of slow crack growth [2], leading to a time dependence of strength. The slow crack growth also appears to be largely independent of the environment [2] and is thus an intrinsic property of the material. The mechanism of slow crack growth is, most likely, associated with plastic processes occurring in the vicinity of the crack tip (see Appendix 3). This plasticity is, in turn, probably related to the viscosity of the amorphous second phase material that forms at grain boundaries during hot-pressing [2].

Slow crack growth processes are normally characterized by the crack velocity, v, and the stress intensity factor, K_I, and the relation between these can be used to evaluate all of the important time parameters needed for failure prediction [3-6]. It is intended in this paper to establish that the slow crack growth process in silicon nitride can be characterized in this way. The relations obtained are then used for failure prediction and, hence, the evaluation of safe working stress levels.

2. The application of fracture mechanics

For a linearly elastic material, the spatial distribution of stress around a crack is determined by the stress intensity factor, K_I, such that σ_{xx}, for example, is given by [7]

$$\sigma_{xx} = \frac{K_I}{(2\pi r)^{1/2}} f(\theta) \qquad (1)$$

where r is the distance from the crack tip and $f(\theta)$ is an angular dependence. The stress intensity factor is also related to the applied stress, σ, and the crack length, a, by

$$K_I = \sigma Y a^{1/2} \quad (2)$$

where Y is a geometric parameter.

When fracture is accompanied by gross plastic deformation, these relations cannot normally be used. For a linearly visco-elastic material, however, the elastic results can be used for stress boundary conditions (since the elastic constants do not enter into the relation for the stress distribution), with σ and K_I becoming time dependent[7-9]

$$K_I(t) = \sigma(t)\ Y[a(t)]^{1/2} \ . \quad (3)$$

The result expressed in Equation 3 has been verified rigorously for a static crack, but is also expected to apply without significant modification to a moving crack [9].

In silicon nitride at elevated temperatures, fracture is accompanied by gross plastic deformation. Fortunately, to a good approximation, the deformation is linearly visco-elastic, i.e., the stress exponent for plastic deformation is ~ 1.5 [10]. It will thus be a good approximation to use the conventional fracture mechanics notations to describe high temperature crack propagation in silicon nitride (noting that K_I is expected to exhibit some time dependence).

3. Fracture mechanics measurements

A full characterization of fracture when crack growth occurs requires, at least, simultaneous measurements of the crack velocity and stress intensity factor. This can be achieved with polycrystalline ceramics in the linearly elastic regime from the rate of load relaxation at constant displacement using a constant K specimen (such as the double torsion specimen). When gross plastic deformation accompanies crack propagation, however, load relaxation owing to plastic flow occurs and it is prohibitively complex to separate the rates of relaxation owing to plastic flow and crack growth. An alternative method for measuring crack propagation rates is thus required. A suitable technique is described in this section, utilizing the properties of a constant K specimen at constant displacement rate.

3.1. Crack propagation rates

For a constant K specimen, the elastic displacement, y_{el}, is related to the applied load, P, and the crack length, a, by [4]

$$y_{el} = P[Ba + C] \quad (4)$$

where B and C are constants which depend only on the specimen dimensions and elastic constants. For an additional plastic displacement, y_P, Equation 4 is still a good approximation for the elastic displacement, when y_P is small (see Appendix 1). The total displacement, y, is thus given by

$$y = y_P + y_{el} = y_P + P[Ba + C] \ . \quad (5)$$

Differentiating Equation 5 with respect to time, t, to obtain the crack velocity gives

$$\frac{da}{dt} = \frac{\dot{y} - \dot{y}_P - (Ba + C)(dP/dt)}{BP} \cdot \quad (6)$$

For a fully elastic specimen tested at a constant displacement rate, (Appendix 2), the load quickly increases to a constant value once the crack starts to propagate. Putting $dP/dt = 0$ in Equation 6, therefore, shows that the crack propagates at constant velocity, with the velocity given, by $da/dt = \dot{y}/BP$.

When plastic displacements occur, the plastic displacement rate is expected to be a function of both load and crack length,* such that, in general,

$$y_P = \mu F(P, a, t) \quad (7)$$

where μ is a proportionality constant. Substituting y_P in Equation 5 and differentiating gives

$$\frac{\partial P}{\partial t} = \frac{\dot{y} - PB(da/dt) - \mu(\partial F/\partial t) - \mu(\partial F/\partial a)(da/dt)}{Ba + C + \mu(\partial F/\partial P)} \cdot$$

In order to obtain a plateau behaviour, $\partial P/\partial t$ must be zero for all a, and hence

$$\mu \frac{\partial F}{\partial t} + \mu \frac{\partial F}{\partial a}\frac{da}{dt} = y - PB\frac{da}{dt} \cdot \quad (9)$$

The crack growth rate, da/dt, is a unique function of K (and hence P) during slow crack growth. Thus, the left hand side of Equation 9 must be constant for all a, if plateau behaviour is

*This can easily be substantiated for the double torsion specimen by measuring plastic displacement rates at one end of a rectangular torsion bar which is rigidly supported at the opposite end. The rate is observed to depend on the length of the bar (equivalent to the crack length for this specimen, see Fig. 2).

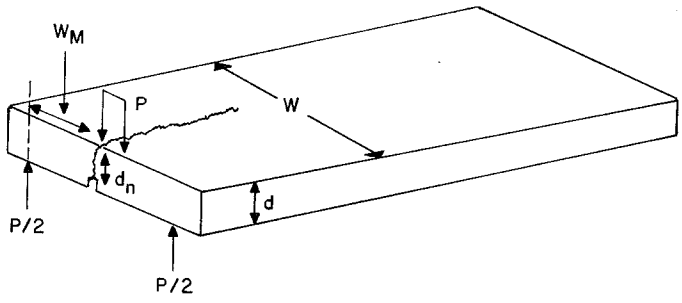

Figure 2 A schematic representation of the double torsion specimen containing definitions of the dimensional parameters.

to be observed when plastic displacements occur. The deformation rate term $(\partial F/\partial t)_{P,a}$ is constant under steady state deformation conditions for given a, but this rate cannot be the same for all a because changing the crack length essentially corresponds to a change in length of the torsion bar subject to plastic displacement. It is a very unlikely combination of properties, therefore, that will yield a crack length independent value for the left hand side of Equation 9 at significant plastic displacement rates. It is thus concluded that the onset of non-plateau behaviour in a constant displacement rate experiment corresponds, in general, to the onset of significant plastic contributions to the total applied displacement.

Some preliminary measurements at constant displacement rate will characterize the load ranges where the plastic displacement rate is substantially smaller than the crack growth displacement rate. Then the crack growth rate, within the valid (plateau) range, can be obtained using the relation; $da/dt = \dot{y}/BP$, with B obtained analytically (see [11]) or empirically.* It is not necessary to use one specimen for each measurement, several values can be obtained on the same specimen by changing the displacement rate once the load plateau is established (see Fig. 4).

3.2. Stress intensity factor

The stress intensity factor for a constant K specimen depends only on the load, P, and the specimen dimensions. The simplest constant K specimen and probably the only one that is suitable for measurements at high temperatures (above 1000° C) is the double torsion specimen. The stress intensity factor for this specimen is given by [11]

$$K = PW_m \left[\frac{3(1+\upsilon)}{Wd^3d_n}\right]^{1/2} = AP \qquad (10)$$

where υ is Poisson's ratio and W, W_m, d and d_n are specimen dimensions shown in Fig. 2.

4. Determination of crack growth rates

The equipment used for high temperature double torsion testing is shown in Fig. 3. The loading device is made from hot-pressed silicon carbide which minimizes plastic displacements at the load application points. The specimen is supported at one end only; hence, in order to retain the specimen in the correct position, without overloading, a load cycling attachment is operated while the enclosure temperature is raised to the test temperature. This cycling attachment comprises essentially of lower and upper load limits which are set to an appropriate load range.

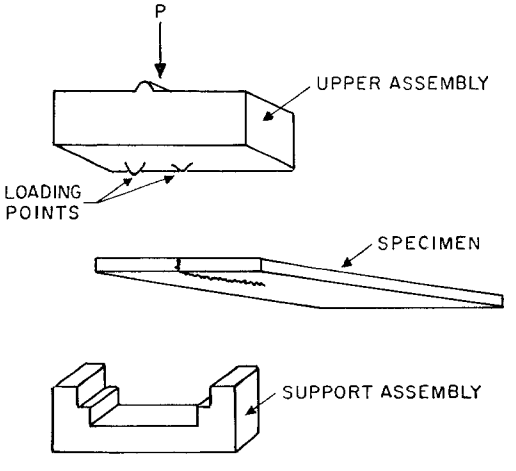

Figure 3 An exploded diagram of the loading assembly used for high temperature crack growth rate measurements.

*Obtained by measuring the time taken for a crack to propagate along the length of a specimen at constant velocity in a constant displacement rate experiment.

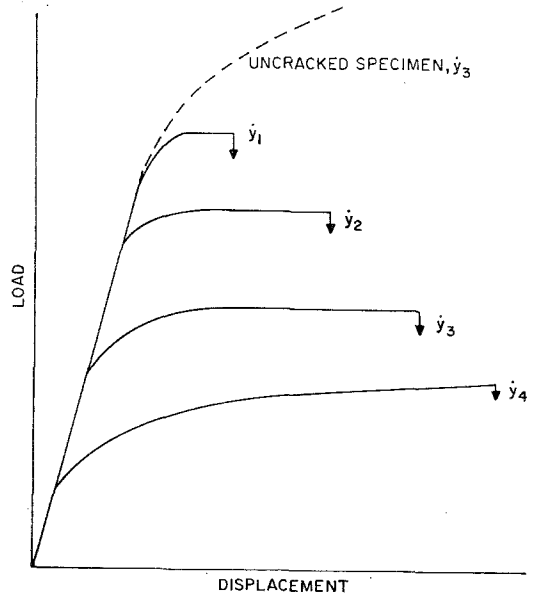

Figure 4 Typical load displacement behaviour observed with silicon nitride at constant displacement rate.

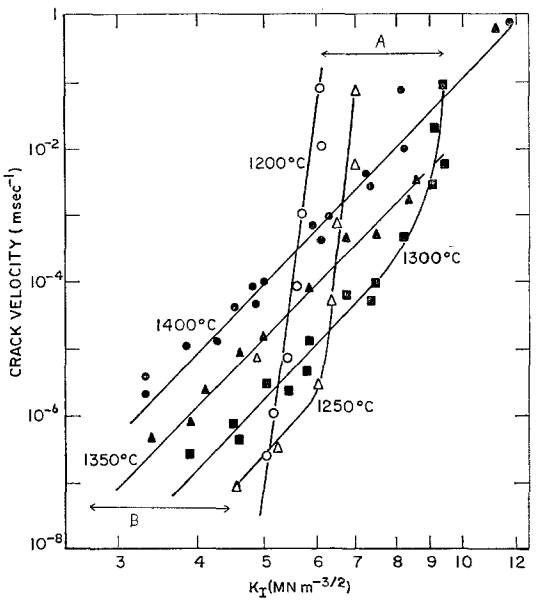

Figure 5 Crack growth rate data obtained for hot pressed silicon nitride at elevated temperatures.

Preliminary experiments on cracked and uncracked specimens to characterize the load range for effective fracture mechanics measurements result in load displacement behaviour of the type shown schematically in Fig. 4. At the higher loading rates ($\dot{y}_1$, $\dot{y}_2$, $\dot{y}_3$) load plateaux are obtained, substantially below the load needed for plastic deformation in an uncracked specimen. It is, thus, quite valid to use load measurements within this range to obtain fracture mechanics data. At the lowest displacement rate, $\dot{y}_4$, plateau behaviour is not obtained and it is not strictly valid to calculate fracture mechanic parameters from the data. Approximate values (which are sometimes good enough to establish trends in the crack propagation rate) can be obtained, however, by measuring the total plastic displacement imposed on the specimen after fracture is complete. Then an average value for the displacement rate, $\dot{y}_P$, can be obtained, which gives an average value for the crack velocity, from Equation 6

$$\frac{d\bar{a}}{dt} = \frac{\dot{y} - \dot{y}_P}{BP} \qquad (11)$$

where $\bar{P}$ is the mean load for crack propagation.

The stress intensity factor, crack velocity data obtained in this way for a commercially available hot pressed silicon nitride* are plotted in Fig. 5. Two distinct behaviours are apparent, designated regions A and B. The region of slowly varying velocity, which occurs in the low velocity range for any given temperature, classified here as region B, is characterized by an essentially constant slope, n (of magnitude 10 ± 2), with K_I decreasing as the temperature is increased. The region of rapidly varying velocity in the high crack velocity range, region A, has a much steeper slope and K_I increases as the temperature increases, as reflected by a rapid increase in K_{IC} at the higher temperatures (Fig. 6).

One additional characteristic of crack propagation in region A which is not summarized in Fig. 5 is the intermittency of the process. It is generally observed that K_I must be increased above the value given in Fig. 5 before the crack will start to propagate, but once moving, it will continue to move in accordance with the K_I-V relation depicted in the diagram. A schematic representation of this behaviour is shown in Fig. 7.

5. Failure prediction

The crack propagation data in Fig. 5 can be used directly for failure prediction. In particular, the minimum time to failure can be predicted after the weakest components have been eliminated by flaw detection procedures, such as proof

*Norton Company HS 130 material was used in order to relate the data to existing strength and creep data.

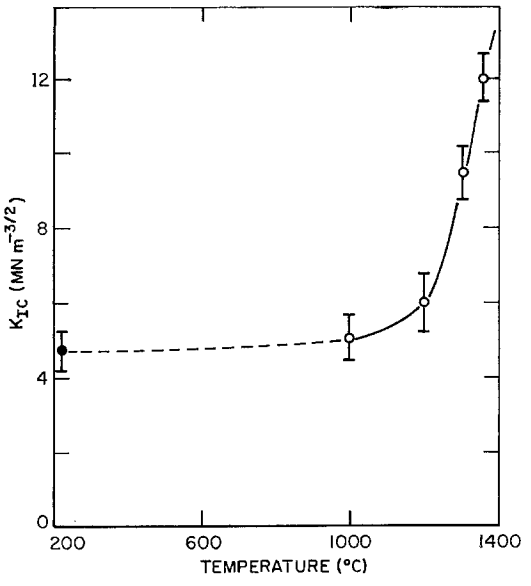

Figure 6 The temperature dependence of K_{IC} for hot-pressed silicon nitride.

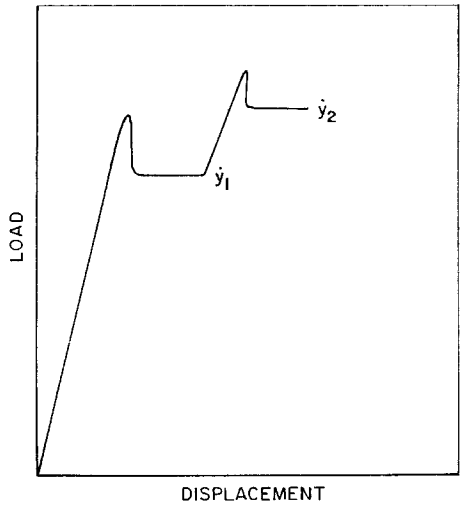

Figure 7 A typical load, displacement record obtained in region A, at high crack velocity, showing the load drop that occurs once the crack starts to propagate.

testing. The time to failure predicted from the crack propagation data is given by [6]

$$\tau = \frac{2}{\alpha\,(n-2)\,\sigma_a{}^2\,Y^2}\left[\frac{1}{K_{Ii}{}^{n-2}} - \frac{1}{K_{IC}{}^{n-2}}\right] \quad (12)$$

where α and n are crack propagation constants (see Appendix 2), σ_a is the applied stress and K_{Ii} is the initial stress intensity factor. Proof testing gives a maximum possible value of $K_{Ii} = K_{IC}(\sigma_a/\sigma_P)$, where σ_P is the proof stress.* Substituting for K_{Ii} gives the minimum time to failure [6]

$$\tau_{min} = \frac{2}{\alpha(n-2)\,\sigma_a{}^2\,Y^2 K_{IC}{}^{n-2}}\left[\left(\frac{\sigma_P}{\sigma_a}\right)^{n-2} - 1\right] \cdot \quad (13)$$

The proof test (or flaw detection) procedure can be conducted at room temperature because the same flaws control the strength both at room temperature and at elevated temperatures (see below, Fig. 10); hence, the ambient temperature value for K_{IC} may be used to evaluate τ_{min}. The minimum failure times predicted by substituting the crack propagation data into Equation 13 (for various (σ_P/σ_a) at 1400°C and for various temperatures at $(\sigma_P/\sigma_a) = 2.0$) are shown in Figs. 8 and 9.†

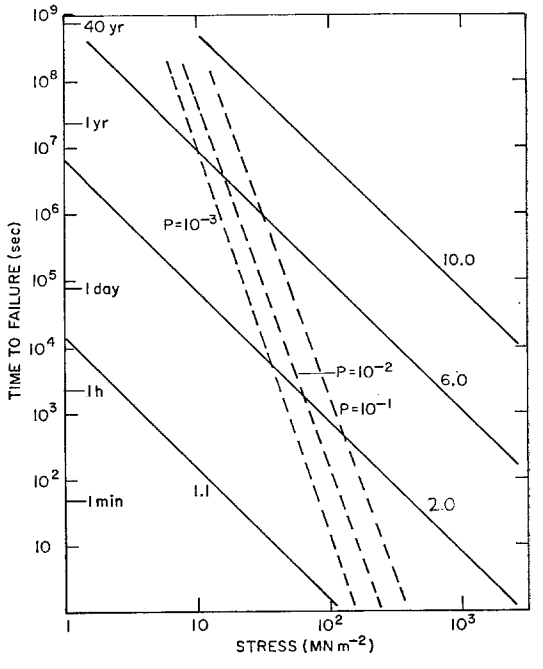

Figure 8 A proof stress diagram for hot-pressed silicon nitride at 1400°C, showing the minimum time to failure as a function of applied stress. The dotted lines are approximate values for the time to failure without proof testing for various failure probabilities.

*Or the stress to extend the largest flaw that can exist below the limits of detection, if non destructive testing is used.
†It is assumed in developing these diagrams from the crack velocity data that there is no substantial change in the form of the V, K_I relation at low crack velocities. This may be quite invalid, of course, and some caution should be exercised in applying the diagrams to long failure times until low velocity data are obtained.

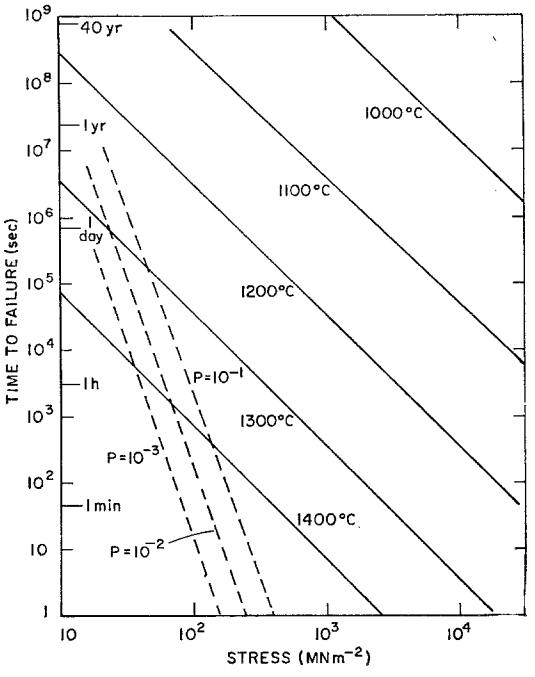

Figure 9 A proof test diagram showing minimum time to failure conditions for various temperatures at a proof stress, applied stress ratio of 2:1.

Also shown on the proof test diagrams are approximate values for the failure times that would be expected without proof testing, τ_0, computed from tensile strength data for silicon nitride [17]. For applications where failure times larger than τ_0 are required, proof testing is an essential pre-requisite to component application; whereas, for lower acceptable failure times, proof testing is redundant. Also, to a first approximation, the failure stresses at $\tau_0 = 1$ sec represent the strength capacity of the material and, therefore, give values for the maximum acceptable proof stress. The diagrams thus contain all of the information that is needed to assess the safe working stress levels for silicon nitride, and whether these can be achieved by proof testing with an acceptable number of proof test failures.

The development of the proof test diagram from the crack propagation data is based on the assumption that the flaws that lead to fracture are pre-existing and similar to the flaws that lead to fracture at ambient temperatures. If this is not true, the diagrams give a conservative estimate of failure times. The validity of the assumption can be shown, however, by predicting the stress rate dependence of the strength from the crack propagation data and comparing this with measured strengths. The stress rate dependence of the strength σ_f is given by [5]

$$\sigma_f = \frac{K_0}{Y(a_0)^{1/2}}\left[1 + \frac{2Y\dot{\sigma}(n+1)\,a_0^{3/2}}{V_0 K_0 (n-2)}\right]^{1/(n+1)} \quad (14)$$

where a_0 is the initial crack length, $\dot{\sigma}$ is the applied stress rate and K_0 and V_0 are values for K and V at the onset of slow crack growth. Substituting the room temperature strength, $\sigma_s[= K_{IC}/Y(a_0)^{1/2}]$, which is independent of stress rate, and rearranging gives;

$$\sigma_f^{n+1} = \frac{2\dot{\sigma}\,(n+1)}{aY^2\,(n-2)}\left(\frac{\sigma_s}{K_{IC}}\right)^{n-2}. \quad (15)$$

Using a median value for the room temperature flexural strength* of 66000 psi† [2] the loading rate dependence of the strength is predicted at 1100 to 1400°C. The predicted strengths are plotted in Fig. 10, where they are compared with measured strengths [2]. The agreement is excellent, confirming that fracture is primarily propagation controlled and occurs from the same

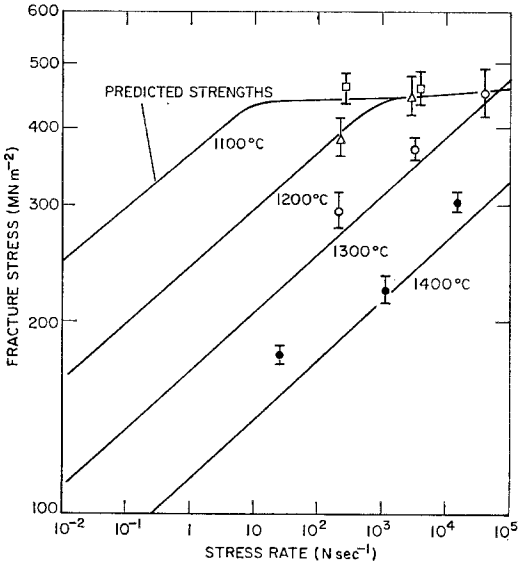

Figure 10 A comparison of the stress rate dependence of the strength predicted from the crack growth rate data with experimental data obtained by Lange in four point flexure (parallel to the hot-pressing direction) for similar material.

*Four point bending, in an orientation parallel to the hot-pressing direction. The difference in testing mode and orientation explains the discrepancy in strengths compared to the data in Fig. 1.
†10^3 psi = 6.89 N mm^{-2}.

flaws that control the ambient temperature strength.

5.1. Application

It is interesting to apply the proof test diagrams to a specific structural problem. An application of considerable current interest is the use of ceramic components in gas turbines. A typical design for a power generating turbine specifies the following conditions for the stator blades; the peak stress occurs during on/off transients at a level of 250 MN m^{-2} for ~ 10 sec at $\sim 1100°C$; the long term stress owing to gas pressure, etc is ~ 35 MN m^{-2} and must be applied for several thousand hours at 1400° C to satisfy the maximum expectation for this component. For a total time to failure prediction the crack growth owing to both stresses must be superimposed, but for the purposes of this simple illustration they are considered separately. At 1100°C very little slow crack growth occurs and a proof stress ratio of only 1:1 ($\sigma_P = 280$ MN m^{-2}) will ensure that the component will survive 10^4 cycles (i.e., a total time of $> 10^5$ sec), at a stress of 280 MN m^{-2}. The performance at 1400°C is much more critical and the proof stress diagram (Fig. 10) shows that at a stress of 35 MN m^{-2} a lifetime of 10000 h can only be ensured if components are proof tested at ten times the service stress (i.e., 350 MN m^{-2}). At this stress, a large proportion of the component will break in the proof test. A more reasonable life expectation for this material under these conditions is thus 1000 h, because this can be ensured using a 6:1 proof stress, which would break only a small proportion of the components during the proof test.

Finally, it is emphasized that these predictions are based on the extrapolation of the data to crack velocities which are several orders of magnitude lower than the measured values; this extrapolation may be invalid, and the diagrams should, therefore, be regarded only as indications of performance until additional low velocity data are obtained.

6. Conclusions

1. A technique for evaluating crack propagation rates in ceramic materials at high temperatures is described. The technique essentially uses a constant K specimen, such as a double torsion specimen, under constant displacement rate conditions.

2. Crack propagation data obtained for hot-pressed silicon nitride using this technique show two regions of behaviour. At high velocities, K_I increases as the temperature is increased; whereas at low velocities, K_I decreases as the temperature increases. The high velocity effect is probably associated with crack blunting, while at low velocities subcritical crack extension is promoted by the formation of grain-boundary sliding cracks.

3. The crack propagation data are used to develop proof test diagrams which give values for the safe working stress levels for silicon nitride after proof testing. An example of the use of these diagrams is also presented.

Appendix 1

Compliance measurements in a plastically deformed double torsion specimen

The effective use of the double torsion specimen for fracture mechanics measurements, when crack growth is accompanied by gross plastic deformation, requires that the elastic compliance should be linearly related to the crack length when small plastic displacements occur (see Equation 4). Whether this applies can be determined experimentally by systematically varying the plastic displacement, y_P, and measuring the elastic compliance. Data of the type obtained for glass samples (where the plastic displacements are applied above the annealing temperature) are shown in Fig. 11 for $y_P \gtrsim y_{el}$. It is noted that the plastic displacement does not have a significant effect on the elastic compliance within this range of y_P/y_{el} ($\gtrsim 1$). The specimen can thus be used for fracture mechanics measure-

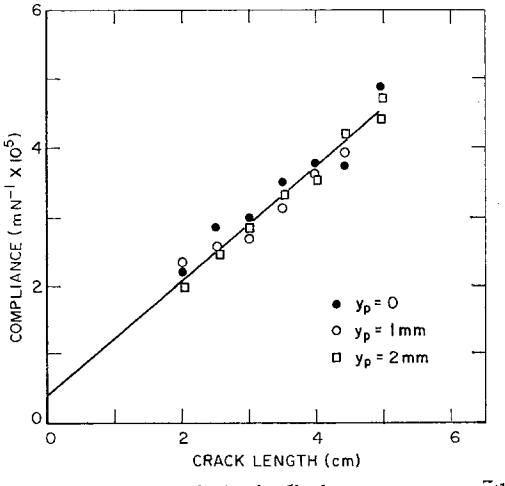

Figure 11 The effect of plastic displacement, y_p, on the compliance of glass plates 1 mm thick.

ments provided that the plastic displacement is small.

Appendix 2

Crack propagation at constant displacement rate

For a constant K specimen in the elastic regime, Equation 6 shows that

$$\frac{da}{dt} = \frac{\dot{y} - (Ba + C)\,\partial P/\partial t}{BP} \cdot \quad \text{(A1)}$$

Also, as shown in Equation 10, P is proportional to K. The crack growth rate during slow crack growth is uniquely related to the stress intensity factor such that [5, 6]

$$\frac{da}{dt} = \alpha K_I{}^n \quad \text{(A2)}$$

where α and n are system constants. Substituting for P and (da/dt) in Equation A1 gives

$$\frac{da}{a} = \frac{\alpha B}{A}\left(\frac{K_I{}^n}{\dot{y} - (\alpha B/A)\,K_I{}^{n+1}}\right) dK_I \quad \text{(A3)}$$

Integration gives,

$$(n + 1)\ln a = -\ln[\dot{y} - (\alpha B/A)\,K_I{}^{n+1}] + \text{constant} \cdot \quad \text{(A4)}$$

Since $K_I = 0$ when $a = a_0$ (the initial crack length)

$$K_I{}^{n+1} = \frac{A\dot{y}}{B\alpha}\left[1 + \left(\frac{a_0}{a}\right)^{n+1}\right] \cdot \quad \text{(A5)}$$

Since n for ceramic materials is generally a large number (>8) K_I increases rapidly to an asymptote, K_{max}, of

$$K_{max} = \left(\frac{A\dot{y}}{B\alpha}\right)^{1/(n+1)} \cdot \quad \text{(A6)}$$

A load plateau, $P_{max} = (K_{max}/A)$, is thus obtained during crack propagation for a constant K specimen tested at constant displacement rate. The magnitude of the plateau depends on the specimen dimensions, elastic properties and the displacement rate.

Appendix 3

Crack growth mechanisms

It is intended to develop the crack growth mechanisms in detail in a separate publication, but a cursory discussion is useful at this stage.

In region A, at high velocities (Fig. 5), the principal feature is the rapid increase in K_I between 1200 and 1400°C. The extent of the slow crack growth is limited and is typical of the visco-elastic growth observed, for example, in glass near the annealing temperature. The origin of the increase in K_I is almost certainly associated with the onset of viscous deformation in the amorphous phases (see below), and the intermittent nature of the crack growth suggests a time/stress dependent crack blunting process. The most likely candidates are (a) blunting owing to grain-boundary sliding (Fig. 12a) or (b) an enhanced grain pull-out contribution to the crack propagation stress (Fig. 12b). The latter is due to the elongated nature of many of the grains [12]; which can result in a pull-out contribution to K_I analogous to that observed in fibre composites.*

In region B, at low crack velocities, crack growth enhancement occurs. The separation of

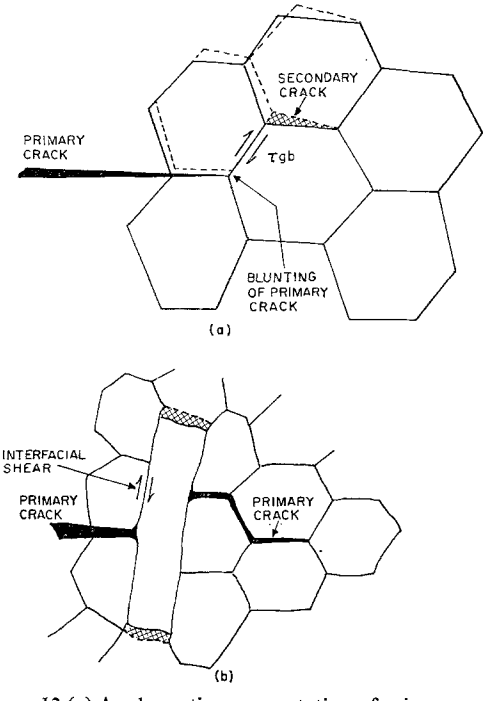

Figure 12 (a) A schematic representation of primary crack blunting and secondary crack formation due to grain-boundary sliding. (b) A schematic representation of the "pull-out" contribution to the stress intensity factor.

*The magnitude of pull-out contributions to K_I depend on the shear strength of the interface with the matrix and reaches a maximum at a critical value of this shear strength [13]. An increase in the pull-out contribution as the temperature is raised could thus occur due to the reduction in the viscosity of the grain-boundary phase, tending towards the critical value.

the velocity curves in this region is indicative of an activated process. If it is considered that the activated process is in the form of a stress dependent activation, then the crack velocity can be expressed in the form

$$V = V_0 K_I^{nT/T_0} \exp\left[\frac{-\Delta H}{RT}\right] \qquad \text{(A7)}$$

where ΔH is the activation enthalpy, T_0 is a temperature-related constant and V_0 is a frequency-dependent constant. The data in region B can be fitted with a good accuracy to this relation and gives an activation enthalpy of 220 kcal mol^{-1}. This value is much larger than the activation enthalpies typically involved in chemical reactions so that the slow crack growth is unlikely to be an environmentally controlled stress corrosion process (consistent with the observation of slow crack growth in an inert environment) [2]. Activation enthalpies of this order can, however, be obtained for viscosity or diffusion, suggesting that the slow crack growth is related either to the onset of viscosity in the amorphous phases or to vacancy condensation at the crack tip [15]. The latter process is expected to be continuous and should occur in single phase amorphous materials. The crack growth is, however, intermittent as manifested by acoustic emission measurements [16], and is not observed in glasses. It is more likely, therefore, that the crack growth is associated with the onset of viscosity, as manifested by grain boundary sliding. The sliding process may, for example, initiate cracks ahead of the primary crack, as depicted in Fig. 12, leading to stress enhancement at the primary crack, which enables crack propagation to occur at $K_I < K_{IC}$.

Acknowledgement

The authors wish to thank the Aeronautics Research Lab, Wright Paterson Air Force Base for their support of this work.

References

1. See for example, F. F. LANGE, ASTM Publication 72-GT-56, New York (1972).
2. F. F. LANGE, *J. Amer. Ceram. Soc.* to be published.
3. S. M. WIEDERHORN, *ibid* **56** (1973) 227.
4. A. G. EVANS, *J. Mater. Sci.* **7** (1972) 1137.
5. *Idem, Int. J. Frac. Mech,* to be published.
6. A. G. EVANS and S. M. WIEDERHORN, NBSIR 73-147, March 1973; *Int. J. Frac. Mech.* to be published.
7. See for example, P. C. PARIS and G. C. SIH, ASTM STP 381 (1964).
8. F. A. MCLINTOCK, *Proc. Roy. Soc. (Lond.)* **A285** (1965) 58.
9. W. G. KNAUSS, *Int. J. Frac. Mech.* **6** (1970) 7.
10. R. KOSSOWSKY, unpublished work at Westinghouse Laboratory.
11. D. P. WILLIAMS and A. G. EVANS, *J. Testing and Evaluation*, **1** (1973) 264.
12. F. F. LANGE, *J. Amer. Ceram. Soc.* to be published.
13. D. C. PHILLIPS, *J. Mater. Sci.* **7** (1972) 1175.
14. S. M. WIEDERHORN, "Corrosion Fatigue" (NACE Publication, Houston, 1972) p. 731.
15. R. N. STEVENS and R. DUTTON, *Mater. Sci. Eng.* **8** (1971) 220.
16. A. G. EVANS and M. LINZER, unpublished work at N.B.S.
17. W. FRAZIER, unpublished work at Westinghouse Laboratories.

Received 29 June and accepted 21 August 1973.